J Supercond Nov Magn (2015) 28:487–492
DOI 10.1007/s10948-014-2745-3

ORIGINAL PAPER

Energy Dissipation Mechanisms in Polycrystalline Superconductor $Y_3Ba_5Cu_8O_y$

Y. Slimani · E. Hannachi · A. Hamrita · M. K. Ben Salem · M. Zouaoui · M. Ben Salem · F. Ben Azzouz

Received: 9 June 2014 / Accepted: 23 August 2014 / Published online: 24 September 2014

Abstract The magnet-resistivity measurements of the Y-based $Y_3Ba_5Cu_8O_{18-x}$ superconductor under different magnetic fields ranging from 0 to 200 mT have been carried out to understand the dissipation mechanisms in the resistive transition. Samples were synthesized in air by solid-state reaction method. Three models are employed to investigate the broadening of the resistive transition. The Ambegaokar–Halperin phase slip (AH), thermally activated flux creep (TAFC) models for granular superconductors, and Kosterlitz–Thouless (KT) model describing the vortex–antivortex unbinding for 2D. Phase analysis by X-ray diffraction (XRD) and morphology examination by scanning electron microscopy (SEM) were carried out. The AH and TAFC models cannot explain the whole of the broadening of resistive transition; a small temperature range is not described by these two models. Furthermore, our experimental data shows a good agreement with the KT model over the entire transition range justifying the picture of vortex–antivortex unbinding.

Keywords $Y_3Ba_5Cu_8O_{18\pm x}$ superconductor · Ambegaokar–Halperin phase slip model · Thermally activated flux creep model · Kosterlitz–Thouless model

Y. Slimani · E. Hannachi · A. Hamrita · M. K. Ben Salem · M. Zouaoui · M. Ben Salem (✉) · F. Ben Azzouz
Laboratory of Physics of Materials - Structures and Properties, Department of Physics, Faculty of Sciences of Bizerte, University of Carthage, 7021 Zarzouna, Tunisia
e-mail: mohamed.bensalem@fsb.rnu.tn

F. Ben Azzouz
Department of Physics, College of Sciences for Girls, University of Dammam, Dammam, Saudi Arabia

1 Introduction

The yttrium-based superconductors family (YBCO) involves several superconducting phases with different zero-resistance temperatures (T_{co}); $YBa_2Cu_3O_{7-d}$ (Y-123) with zero-resistance temperature $T_{co} \approx 90$K, $YBa_2Cu_4O_8$ (Y-124) with $T_{co} \approx 80$K, and $Y_2Ba_4Cu_7O_{15}$ (Y-247) with T_{co} ranging from 30 to 95 K, depending on the oxygen content that were synthesized. Aliabadi et al. [1] have synthesized $Y_3Ba_5Cu_8O_{18-x}$ (Y-358) compound that becomes superconductor at 98 K. The discovery of superconductivity in Y-358 has attracted considerable interest, and some preparation methods have been employed and superconducting transition temperatures ranging from 80 to 98 K have been reported [2, 3]. Y-358 has a crystalline structure similar to that of Y-123 with the exception of the number of CuO chains and CuO_2 planes which exceed those in Y-123. The Y-358 compound has five CuO_2 planes and three CuO chains. Due to the structural resemblance and similarity of the superconducting transition temperature of Y-123 and Y-358, one can encounter some difficulties to distinguish between these compounds. Recently we have reported a comparative study of nanosized particles $CoFe_2O_4$ effects on superconducting properties of Y-123 and Y-358 [4] and we have shown that these compounds exhibit dissimilar behavior.

The broad resistivity transition caused by both external magnetic fields and transport currents has prompted intense research activity to understand the dissipation phenomenon. Various theoretical models involving thermally activated flux creep model [5], Ambegaokar–Halperin (AH) phase slip [6], Kosterlitz–Thouless (KT) transition [7], thermally activated flux flow [8], fluctuations [9], etc. have been proposed in order to interpret the origin of this behavior. Some previous studies have suggested that the problem

of dissipation behavior of the layered superconductors has been achieved by applying the KT theory [7]. Ausloos et al. [10] had interpreted the electrical resistivity behavior in spray-dried bulk $Bi_2Sr_2CaCu_2O_{8+d}$ in terms of a 2D KT theory. Bhalla et al. [11] have also found a reasonable agreement between the KT model and the low resistivity part under magnetic fields for bulk $Bi_{1.6}Pb_{0.4}Sr_2Ca_2Cu_3O_x$. Xu et al. [12] have shown that KT model describes very well the experimental data in granular $YBa_2Cu_3O_{7-d}$. However, other researchers have shown that a unique model is not sufficient to explain this unusual broadening of the transition resistive [13–15]. They have applied the AH phase slip model [16–18] to a medium of Josephson weak links, and they have found a satisfactory agreement between theoretical and experimental data in bulk Bi-2223 superconductor. Additionally, they have recourse to the concept of thermally activated flux creep (TAFC) model proposed by Anderson [19] for the resistivity region near T_{co} and they proved that the vortex dynamics seems to dominate the cause of energy dissipation. Balaev et al. [20] have also discussed the mechanisms responsible for broadening of the resistive transition in composites YBCO + CuO under different magnetic fields, and they have observed a crossover from AH to flux creep model in the intermediate magnetic field range. Other groups [11, 15] have regained the crossover from the phase fluctuation of order parameter to vortex dynamics in bulk YBCO through which they have defined a small range of temperature ΔT^* where both mechanisms seem to be responsible for energy dissipation. On our knowledge, there is only one paper which focuses on the study of the flux dynamic properties in both Y-358 and Gd-358 systems by relying solely on the modified flux creep model [21]. The different regimes of energy dissipation are not widely investigated up to date. The main aim of the present study is to understand the complex dissipation behavior in Y-358 sample by using different theoretical models. So we report an analysis of the physical mechanisms responsible for the broadening of the magnetoresistivity measurements of $Y_3Ba_5Cu_8O_{18-x}$. We show that the AH phase slip model and the flux pinning mechanism induced by TAFC are accounts for the dissipation range of temperature with appearance of a small temperature range in which neither the first nor the second model are directly applicable. The KT model, on the other hand, explains very well our experimental data in the whole of the broadening of resistive transition.

2 Experimental Details

Polycrystalline samples of $Y_3Ba_5Cu_8O_y$ were synthesized by solidstate reaction. Commercially powders $BaCO_3$ (99.9 % purity), Y_2O_3 (99.99 % purity), and CuO (99.9 % purity) were used as starting materials. The powders were mixed according to the chemical formula of Y:Ba:Cu = 3:5:8 by hand grinding in an agate mortar with an agate pestle. The mixed materials pressed into pellets and then calcined for 12 h at 900°C. Calcination step was repeated twice with intermediate grinding. The obtained precursor was pressed into pellets and sintered at 950°C for 48 h in an oxygen atmosphere and then cooled to room temperature at a rate of 4°C/min. The heat treatment processes of sample were performed in alumina crucible.

The structure and phase identification of the powder sample ground from sintered pellets were examined by powder XRD using a Philips 1710 diffractometer with CuK_α radiation. The microstructure of sample was characterized using a scanning electron microscope (JEOL JSM-6390LV). The transport properties of the sample were studied by measuring the electrical resistivity temperature $\rho(T)$ using the four-probe technique. A magnetic field was applied along the short axis of the samples, and the excitation current was injected along the length axis of the samples. The pellets were carefully cut into bar-shaped samples. Electrical contacts were made using silver paint and the contact resistance value was approximately 0.5 Ω. A low excitation current ($I << I_c$: the critical current) is used in order not to affect the behavior of the resistivity transition of samples.

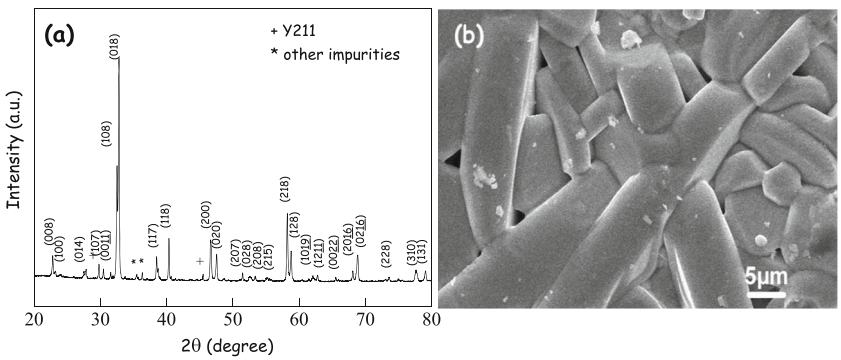

Fig. 1 **a** X-ray powder diffraction patterns of Y-358 sample. **b** SEM micrographs of surface view of the fracture part of Y-358 sample

3 Results and Discussions

Figure 1a shows the powder XRD spectrum of Y-358 sample with designated Miller indices. The analysis of the data denotes a predominately single-phase structure Y-358 with orthorhombic *Pmm2* symmetry. However, small impurity peaks are observed and identified with (*) and (+) on the spectrum. SEM micrograph of the surface morphology of Y-358 sample is shown in Fig. 1b. The microstructure exhibits a plate-like grain with random orientation in all directions. Figure 2 shows the magnetoresistivity measurements of the Y-358 sample under different magnetic fields. It is clear that the applied magnetic field produces a noticeable broadening of the superconducting transition and reduces the temperature at zero resistivity T_{co}. There are two parts in the mixed state of ρ(T, H) transitions curves: A steep part, associating with the superconductivity onset in the intragrains and a lower temperature region characterizing the grain-boundaries network or intergranular effects, which are considered to be weak Josephson type links. Inset of Fig. 2 shows the dependence of the resistive transition width, $\Delta T_{co} = T_c(H = 0) - T_{co}H$ as a function of the applied magnetic field. The transition width is well fitted according to a power-law scaling relation $\Delta T = \alpha H^{-n}$ with n is equal to 0.29 ± 0.03 and the value of the factor α is found to be 1.16 ± 0.02. Such dependence is usually remarkable in the granular superconductors [17, 22, 23]. In the case of Y-123, the parameters n and α are found to be 0.32 ± 0.01 and 1.35 ± 0.03, respectively [24].

Generally, the resistivity transition in the polycrystalline HTS cannot be explained by a unique model [15, 20]. The AH phase slip model could be applicable in high

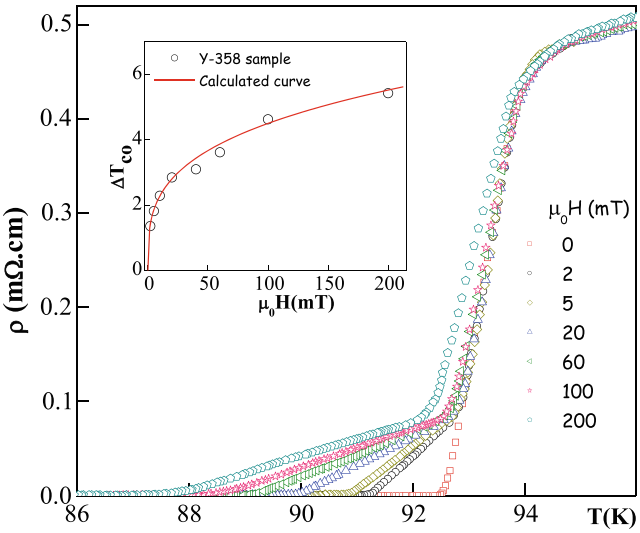

Fig. 2 Variations of the electrical resistivity with temperature at different applied magnetic field of Y-358 sample. *Inset* shows the variation of the transition width ΔT_{co} as a function of the applied magnetic field

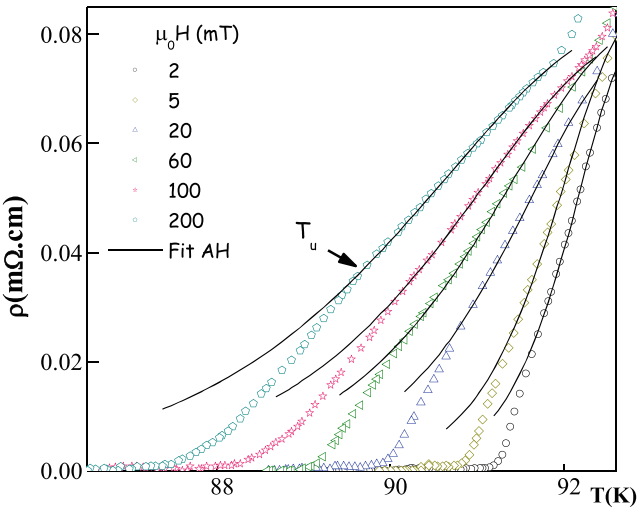

Fig. 3 AH phase slip fit (*lines*) for resistivity versus temperature data (*symbols*) under different applied magnetic fields of Y-358 sample

temperature near T_c where T_c is the peak temperature of the $d\rho/dT$ versus T curve defined as the critical temperature of the superconducting Josephson junction forming. The resistivity ρ(T), given by this approach in the limit of low current, $I << I_c(T)$, is written as $\rho(T) = \rho_0[I_0(\gamma/2)]^{-2}$ [17] where I_0 is the zero-order modified Bessel function [11, 24], ρ_0 is the average normal resistance of the junction, and γ is the normalized barrier height for thermal phase slippage defined as γ(H, T) $= C$(H)(1-t)^q where $t = T/T_p$is the reduced temperature and C(H) is a parameter depending on the magnetic field. Note that T_P is the branching point of the curve. The resistivity curves under magnetic field fitted by AH model for Y-358 sample are represented in Fig. 3. In the fitting process of the resistivity $\rho(T, H)$, we have excluded the regions near the T_c and T_g temperatures (T_g is the glass transition temperature). We started our fitting procedure by considering the experimental values of T_p and ρ_p while the other two parameters CH and q are used as free. It follows that the parameters ρ_p and T_p are substantially unchanged for different magnetic fields. Furthermore the values of the exponent q are around 1 and the parameter CH decreases on increasing the magnetic field (Table 1). For all curves,

Table 1 Values of ρ_p, T_p , CH and q at different magnetic fields for Y-358 sample

$\mu_0 H$(mT)	ρ_p(mΩ cm)	T_p(K)	CH	q
2	0.0789	92.85	219.6	0.96
5	0.0822	92.81	184.5	0.96
20	0.0763	92.82	119.7	0.95
60	0.0803	92.86	87.59	0.93
100	0.0786	92.84	77.65	0.94
200	0.0815	92.83	65.95	0.95

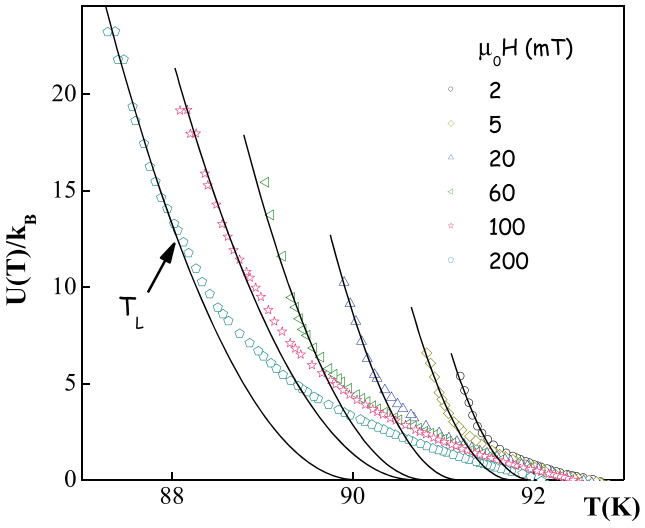

Fig. 4 Temperature dependence of the U(T) at various magnetic fields for Y-358 sample

it should be noted that the AH model describes a fairly large zone of the resistive transition, but it deviates from the experimental data points at temperature T_u. Many authors [13, 15] have reported that the AH model cannot explain adequately all the part of broadened resistivity curves of ρ(T, H), and they suggested that the flux creep model is the preferable regime in the tail part with the exponential relation [5, 26] as: $\rho(T, H) = \rho_p \exp(-U(T, H)/k_B T)$, where ρ_p is the pre-exponential factor independent of the applied magnetic field, k_B is the Boltzmann constant, and U(H, T) is the pinning energy that depends on temperature and magnetic field which expressed as $U(H, T) \approx U(0)(1\text{-}t)^m H^{-n}$, where $t = T/T_c$ is the reduced temperature, $U(0)$ is the effective unperturbed pinning potential at T = 0 K, m and n are taken as fitting parameters. Previously, Anderson et al [27] have demonstrated the field dependence of T_g in HTS: $H = H_o(T_{co} - T_g(H)/T_g H)^{1/n}$. Such relation allows to derive the magnetic field dependence U(H) which can be expressed as $U(H) = (T_{co}/T_g(H) - 1)^{-1}$ and the temperature dependence U(T) which is given by $U(T) = -[k_B T(T_{co} - T_g(H))/T_g(H)] \ln(\rho/\rho_p)$. Typical result of U(T) for Y-358 sample is presented in Fig. 4. It is clear that the form of $U(T) = U(0)(1 - T/T_P)^m$ explains correctly the experimental data for a temperature below T_L.m and T_p parameters were determined from fitting experimental curves. Generally, the temperature exponent, m, is usually chosen to be $m = 2$ [28], 3/2 [29], and 1 [30]. Within the framework of this study, the parameter fitting m is found to be 2 which corresponds to 2D vortex anisotropy state. A same value of m has been reported in the Y-123 embedded with nanoparticles of Y-deficient Y-123, generated by the planetary ball milling [15]. In order to estimate the pinning energy, we have plotted $\ln(\rho/\rho_p)$ versus $(1 - T/T_P)^2/T$ at various magnetic fields. Typical curves are presented in Fig. 5a. From the linear behavior in the tail part below the temperature T_L as indicated by solid line, we have determined the slope of each line which yields the activation energy U(H). Figure 5b shows the variations of UH with applied magnetic field of Y-358 sample. The flux pinning energy decreases with increasing the applied magnetic field, and it is of the order of magnitude of other approaches [31]. We note that the activation energy in Y-358 sample is higher than reported in Y-123 sample [15]. UH can be fitted by a power-law relation: $U(H) \approx H^{-n}$. In our case, the value of the exponent n is 0.57; this is in accordance with reports published earlier [15, 31].

Based on our data, we can conclude that TAFC model describes a restricted zone $\Delta T = T_L - T_g$, i.e., just the lower part. Figure 6 shows the experimental and calculated resistivity ρ(T) for various applied magnetic field of Y-358 sample. Solid and dashed lines correspond to the theoretical curves of AH and TAFC approaches, respectively. It follows that there exists a small range of temperature which is not calculated by these models. The width of the small region $\Delta T^* = T_u - T_L$ versus applied magnetic field ranging from 0 to 200 mT is indicated in inset of Fig. 6. It is clear that the width extends due to the increase in the applied magnetic field.

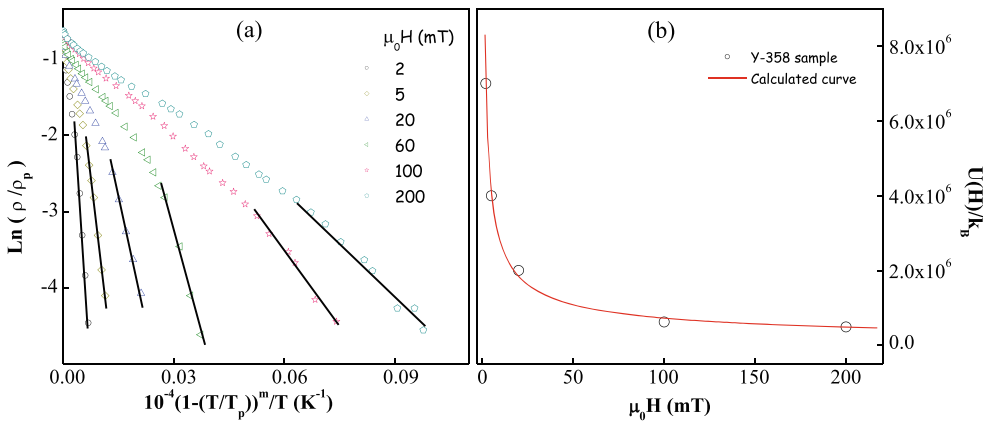

Fig. 5 **a** Plots of the low temperature $\ln(\rho/\rho_p)$ versus $(1 - T/Tp)^m/T$ at various magnetic fields for Y-358 sample. **b** Variations of UH with applied magnetic field for Y-358 sample

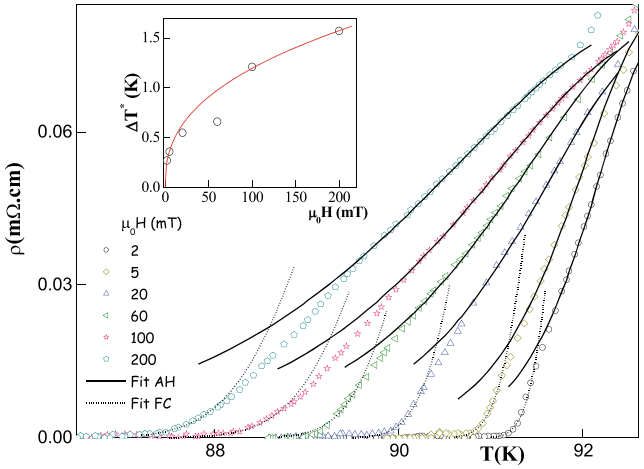

Fig. 6 Dependence of the resistivity as a function of the applied magnetic field for Y-358 sample. *Solid* and *dashed lines* indicated AH and TAFC fits, respectively. *Inset* shows the dependence of the transition region $\Delta T^* = T_u - T_L$as a function of the applied magnetic field

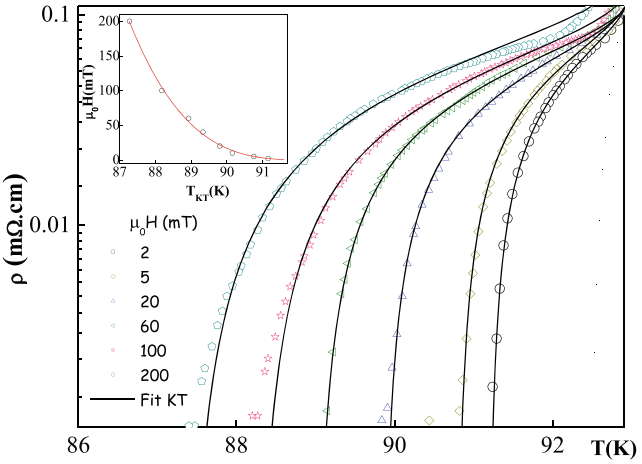

Fig. 7 KT fit (*lines*) for resistivity versus temperature data (*symbols*) of Y-358 sample under different applied magnetic fields. *Inset* shows the variation of the applied magnetic field versus the Kosterlitz–Thouless transition temperature T_{KT}

In the following of this study, we have attempted to consider a model that describes the observed dissipation in the small range which is not described by neither AH nor flux creep models. The Kosterlitz–Thouless transition of vortex–antivortex unbinding because of thermal fluctuation has been proposed and has successfully been applied to analyse experimental results in both bulk and single crystal samples of HTS [32–35]. This model could be applied directly above a temperature called Kosterlitz–Thouless phase transition temperature (T_{KT}) and supposed remains valid until a few degrees below the mean-field (Ginzburg–Landau) transition temperature (T_{GL}). In most reports, T_{GL} fixed as the temperature at which $d\rho/dT$ showed a peak value [38]. Below T_{KT}, there are no free vortices induced by thermal excitation and all of the vortices are frozen into vortex–antivortex pairs. Nevertheless, when the temperature is increased, some parts of the vortex–antivortex pairs will be thermally dissociated into the unbinding vortices, leading to dissipation in the superconductors. In the proximity of T_{GL}, fluctuations of the amplitude of the order parameter are relevant favoring an ohmic behavior of the paraconductivity [37]. According to Halperin and Nelson [38], the resistivity, in terms of the mean free path ℓ and the zero-temperature coherence length ξ_0 follows exponential square root dependence in the dirty limit namely, $\frac{\rho}{\rho_N} = A\frac{\ell}{\xi_0}\exp[-\beta(\frac{T_{GL}-T}{T-T_{KT}})^{0.5}]$, where ρ_n is the normal state resistivity and A and β are nonuniversal constants of the order of unity.

Figure 7 shows KT fits of the resistivity under different magnetic field in semi-logarithmic scale. In the initial fitting procedure of the resistivity $\rho(T, H)$, we take into account the experimental values of T_{GL} and $T_{KT} \sim T_g$, while $\alpha = A\frac{\ell}{\xi_0}$and β were left free. The value of T_{GL} is practically independent of the magnetic field and equals to 92.9 K while T_{KT} shifts to a lower value on increasing the applied magnetic field (inset of Fig. 7). For each curve, the free parameters α and β have been determined from the fit. In our case, $\alpha = 1$ and $\beta = 1.1$. These values are similar to those found by Bhalla et al. [11, 13]. One can note that KT theory describes the phenomena of dissipation in Y-358 sample in the whole of the temperature range $T_{KT} < T < T_{GL}$, the experimental data deviate from the KT model close to T_{KT} and T_{GL} temperatures. Deviation from the linear behavior near T_{GL} may be due to fluctuations in the amplitude of the order parameter. For lower temperatures, the dissipation mechanisms seem to be related to the vortex dynamics.

4 Conclusion

We have analyzed the broadening of the resistive transition in Y-358 compound through the resistivity $\rho(T)$ measurements under applied magnetic fields ranging from 0 to 200 mT. Our results show that the resistivity broadening are described by three dissipation mechanism models, i.e., the Ambegaokar–Halperin model dominated by a phase slip process of the order parameter, thermally activated flux creep model, and Kosterlitz–Thouless theory. The AH model is found to explain the dissipation in the temperature range $T_L < T < T_p$. At low temperatures below T_u, the mechanism of vortex dynamics seems to be predominant. AH and TAFC models. Moreover, TAFC and AH models cannot explain the variation of $\rho(T, H)$ in the temperature range $\Delta T^* = T_u - T_L$. While the KT model explains adequately, our experimental data in the whole of the broadening of resistive transition.

References

1. Aliabadi, A., Akhavan Farshchi, Y., Akhavan, M.: Phys. C **469**, 2012 (2009)
2. Ekicibil, A., Cetin, S.K., Ayas, A.O., Coşkun, A., Fırat, T., Kıymac, K.: Solid State Sci. **13**, 1954 (2011)
3. Topal, U., Akdogan, M., Ozkan, H.: J. Supercond. Nov. Magn. **24**, 2099 (2011)
4. Slimani, Y., Hannachi, E., Ben Salem, M.K., Hamrita, A., Varilci, A., Dachraoui, W., Ben Salem, M., Ben Azzouz, F.: Phys. B **450**, 7 (2014)
5. Palstra, T.T.M., Batlogg, B., van Dover, R.B., Schnee-meyer, L.F., Waszczak, J.V.: Appl. Phys. Lett. **54**, 763 (1989)
6. Ambegakar, V., Halperin, B.I.: Phys. Rev. Lett. **22**, 1364 (1969)
7. Kosterlitz, J.M., Thouless, D.J.: J. Phys. C **6**, 1181 (1973)
8. Tinkham, M.: Phys. Rev. Lett. **61**, 1658 (1988)
9. Kitazawa, K., Kambe, S., Naito, M.: In: Fukuyama, H., Mackawa, S., Malozemoff, A.P. (eds.) Proceedings of IBM Japan Int. Symposium. Springer/Verlag, Heidelberg (1989)
10. Ausloos, M., Bougrine, H., Duvigneaud, P.H., Guo, Y.F.: Phys. C **251**, 337 (1995)
11. Bhalla, G.L., Pratima, A.M., Singh, K.K.: Phys. C **391**, 17 (2003)
12. Ke-xi, X.u., Abbas, A., Essa, J.S.B.: Phys. C **321**, 258 (1999)
13. Bhalla, G.L.: Pratima: Phys. C **406**, 154 (2004)
14. Zouaoui, M., Ghattas, A., Annabi, M., Ben Azzouz, F., Ben Salem, M.: Supercond. Sci. Technol. **21**, 125005 (2008)
15. Hannachi, E., Ben Salem, M.K., Slimani, Y., Hamrita, A., Zouaoui, M., Ben Azzouz, F., Ben Salem, M.: Phys. B **430**, 52 (2013)
16. Tinkham, M., Lobb, C.J.: In: Ahrenreich, H., Turnbull, D. (eds.) Solid State Physics, vol. 42, p. 9132. Academic, New York (1989)
17. Tinkham, M.: Phys. Rev. Lett. **61**, 1658 (1988)
18. Mohammadizadeh, M., Akhavan, M.: Phys. C **30**, 134 (2003)
19. Anderson, P.W., Kim, Y.B.: Rev. Mod. Phys. **36**, 39 (1964)
20. Balaev, D.A., Popkov, S.I., Shaihutdinov, K.A., Petrov, M.I.: Phys. C **435**, 12 (2006)
21. Aliabadi, A., Akhavan-Farshchi, Y., Akhavan, M.: J. Supercond. Nov. Magn. **27**, 741 (2014)
22. Dubson, M.A., Herbet, S.T., Calabrese, J.J., Harris, D.C., Patton, B.R., Garland, J.C.: Phys. Rev. Lett. **60**, 1061 (1988)
23. Mohammed, N.H., Abou-Aly, A.I., Awad, R., Rekaby, M.: Supercond. Sci. Technol. **19**, 1104 (2006)
24. Hamrita, A., Ben Azzouz, F., Madani, A., Ben Salem, M.: Physica C **472**, 34 (2012)
25. Gaffney, C., Petersen, H., Bednar, R.: Phys. Rev. B **48**, 3388 (1993)
26. Kim, J.J., Lee, H., Chung, J., Shin, H.J., Lee, H.J., Ku, J.K. Phys. Rev. B **43**, 2962 (1991)
27. Andersson. M., Rydh, A., Rapp, Ö.: Phys. Rev. B **63**, 184511 (2001)
28. Gross, R., Chaudhari, P., Dioms, D., Gupta, A., Koren, G.: Phys. Rev. Lett. **64**, 228 (1990)
29. Yeshurun, Y., Malozemoff, A.P.: Phys. Rev. Lett. **60**, 2202 (1988)
30. Plastra, T.T.M., Batlogg, B., Van Dover, R.B., Schneemeyer, I.F., Waszczak, J.V.: Phys. Rev. B **41**, 6621 (1990)
31. Wang, Z.H., Cao, X.W.: Solid State Commun. **109**, 709 (1999)
32. Martin, S., Fiory, A.T., Fleming, R.M., Espinosa, G.P., Cooper, A.S.: Phys. Rev. Lett. **62**, 677 (1989)
33. Yeh, N.-C., Tsuei, C.C.: Phys. Rev. B **39**, 9708 (1989)
34. Sugahara, M., Kojima, M., Yoshikawa, N., Akeyoshi, T., Haneji, N.: Phys. Lett. A **125**, 429 (1987)
35. Stamp, P.C.E., Forro, L., Ayache, C.: Phys. Rev. B **38**, 2847 (1988)
36. Ausloos, M., Lanrent, Ch., Patapis, S.K., Rulmont, A., Tarte, P.: Mod. Phys. Lett. B **3**, 167 (1989)
37. Balestrino, G., Livanov, D.V., Montuori, M.: Phys. C **234**, 77 (1994)
38. Halperin, B.I., Nelson. David, R.: J. Low Temp. Phys. **36**, 599 (1979)